Journal of the European Ceramic Society 20 (2000) 1135–1143

Mechanical-property evaluation of thin corroded surface layers of ceramic materials by the microindentation technique

M. Futakawa[a,*], T. Wakui[b], I. Ioka[a], M. Eto[a]

[a]*Department of Nuclear Energy System, Japan Atomic Energy Research Institute, Tokai-mura, Naka-gun, Ibaraki-ken 319-1195, Japan*
[b]*Department of Mechanical Enginnering, Niigata University, Ikarashi Ni-nocho, Niigata-shi, Niigata-ken 950-2181, Japan*

Received 28 June 1999; accepted 14 October 1999

Abstract

An instrumented depth-sensitive microindentation technique was applied to evaluate mechanical properties of thin corroded layers of some ceramics which were immersed in boiling, highly condensed sulfuric acid up to 1000 h. Indentation load–depth curves were analyzed using a finite element model to systematically investigate the effect on the ceramics of film or corroded layer. The mechanical properties of both the oxide films and the corroded layers were evaluated through the combination between analytical and experimental results on the indentation curves. It was found that the relationship between thickness T of oxide films or corroded layers and the depth d determined by the slope change on the indentation load/depth–depth curve is described as $T \approx 10d$. The bending strengths of Si_3N_4 and Al_2O_3 after immersion were evaluated using the d associated with the corroded layer thickness and the K_{IC} obtained before immersion. It was confirmed that the strength degradation of Si_3N_4 and Al_2O_3 due to the boiling sulfuric acid corrosion can be estimated using K_{IC} and d-value.

Keywords: Al_2O_3, Corrosion; Mechanical properties; Identation; Si_3N_4; Surfaces

1. Introduction

A thermochemical hydrogen production system, iodine-sulfur (IS) process investigated by the Japan Atomic Energy Institute,[1] consists of chemically active environments, i.e. boiling sulfuric acid and halogen gasses, in which most of the conventional structural materials are attacked by corrosion.[2] It is a key issue to find appropriate corrosion-resistant materials for proceeding to a next stage, the scaled-up IS process.

Generally, it is known that some ceramics exhibit a good corrosion resistance due to their chemical inertness,[3] while their strengths are influenced by the surface condition because of their brittleness sometimes causing unexpected fracture. The presence of micron-order flaws on the surface aggravates the integrity of ceramic materials.[4] Some engineering ceramics have, therefore, been examined for their corrosion resistance against the boiling highly condensed sulfuric acid. After an immersion test up to max. 1000 h, the corrosion resistance was evaluated by mass change, bending strength and macro- and microscopic observation. In addition, a depth-sensitive microindentation technique was applied to evaluate mechanical properties of the corroded surface layers. An inverse analysis on the load–depth relationship obtained from the microindentation technique was carried out by using an FEM code to qualitatively determine the properties of the corroded surface layer, associated more strongly with the strength degradation in the ceramics rather than the mass change which was conventionally used to evaluate corrosion resistance in the metals. In this paper, not only the corrosion behavior of the ceramics in the boiling, highly condensed sulfuric acid, but also a novel technique to nondestructively estimate the corroded thickness which influences the strength degradation are reported.

2. Experiment

2.1. Materials

Ceramic materials used in the test are reaction-bonded silicon carbide containing about 10% free silicon:

* Corresponding author. Tel. : +81-29-282-5363; fax: +81-29-282-6489.
E-mail address: futakawa@popsvr.tokai.jaeri.go.jp (M. Futakawa).

0955-2219/00/$ - see front matter
PII: S0955-2219(99)00283-6

Si–SiC, pressureless sintered silicon carbide with additives of C and B: SiC, pressureless sintered silicon nitride with additives of SrO, MgO and CeO_2: Si_3N_4, partially stabilized zirconia Y-PSZ with Y: ZrO_2, 93% alumina: Al_2O_3. They are widely used as engineering ceramics. The size of the specimens was $3\times4\times40$ mm^3, which is a measurable size of three-point bending strength.

2.2. Immersion test

The test solution was 95 mass% sulfuric acid. The test was performed in a pyrex glass flask with a capacity of 1 dm^3. The flask was heated in a mantle heater to maintain a stable boiling condition: the temperature was set about 320°C in an ambient atmosphere. Evaporated sulfuric acid solution was liquefied in a reflux condenser to minimize the evaporation loss. The immersion period was 10, 100, 1000 h, and the test solution was not refreshed during the immersion test. The immersion period was defined as the time between the moment boiling began and the moment when the heater was shut down. After the solution's temperature decreased to the ambient temperature, the specimen was removed from the solution and washed by splashing water on it. Then it was washed ultrasonically in water for 5 min.

2.3. Mechanical property evaluation test

The three-point bending strength σ (JIS R 1601) was measured at room temperature after and before immersion. Also, mass M and hardness H were measured before and after the immersion test. The hardness was obtained using a Vickers indenter from the depth under the indent load P of 98 and 980 mN, given by:

$$H = P/Ch^2 \quad (1)$$

where C is constant related with the shape of indenter (e. g. $C = 26.43$ for the Vickers indenter). Toughness of the ceramics K_{IC} was measured by controlled surface flow (CSF) and/or single edge-precracked beam (SEPB) methods[5] before the immersion test using the specimen which was annealed at 800°C for 2 h to remove a residual stress after precracking by the Vickers indenter. The number of specimens of each ceramic with each immersion period is 10 for the strength, mass and toughness measurements. The hardness was measured using 4 specimens for each experimental condition and at 15 points per one specimen. Table 1 shows mean values before the immersion test.

In addition, the depth-sensitive microindentation test was carried out to evaluate the mechanical properties of the corroded surface layer. A depth–load curve is recorded during an indent loading. Maximum indent load is 980 mN. The indentations at this load were crack free, which is a requisite for meaningful hardness and Young's modulus evaluation. It is well known that the slopes of the load/depth against the depth during loading, A, and during unloading, B, shown in Fig. 1, are proportional to the hardness and the Young's modulus, respectively.[6] Thus, it is possible to estimate these properties directly from the load/depth–depth relationship in the case of the homogeneous materials. The measured load–depth behavior is believed to be influenced by the thin surface layer that may be attacked by the corrosion. The effects of the corroded layer and the interaction between the corroded layer and the substrate would appear on the load–depth curve.

The specimen surface and cross-section were inspected by SEM and EPMA (point and line analyses) to determine the corroded thickness.

Table 1
Measured mean values for each ceramic before immersion test

	M_0 (g)	σ_0 (MPa)	H_0 (MPa)	K_{IC} (MPa m$^{1/2}$)
Si–SiC	1. 4	280. 0	13	3. 7[a]
SiC	1. 5	476. 7	14	2. 6[b]
SI_3N_4	1. 6	1194	11	6. 3[a], 6. 2[b]
Al_2O_3	1. 9	333. 5	17	3. 8[b]
Y-PSZ	2. 9	1097		

[a] SEPB.
[b] CSF.

3. FEM analysis on microindentation test

The interaction between scales, corroded layers and substrates complicates the deformation under the indenter and makes it difficult to characterize the corroded layer. The inverse analysis on the measured load/depth–depth curve was performed using an explicit FEM code DYNA,[7] which enables us to analyze a large deformation, to determine mechanical properties of the corroded layer and interprete on the complicated load–depth relationship. In this analysis, the indenter and specimen are treated as

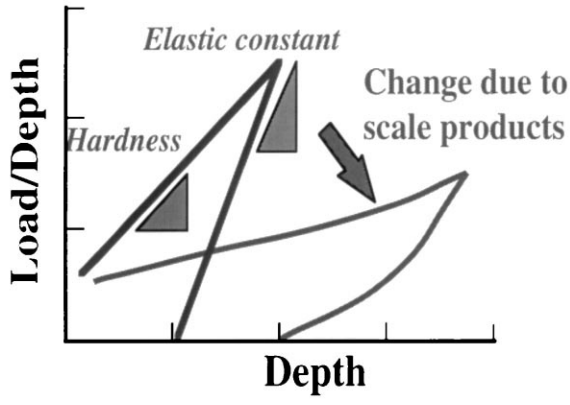

Fig. 1. Schematic drawing of load/depth–depth curve.

axisymmetric two-dimensional bodies taking account of the calculative efficiency. The Vickers indenter used in the experiment was modeled to be a conical tip, which has the same ratio of the depth to a displaced volume as Vickers and Berkovich tips. Although the discrepancy between the axisymmetric two-dimensional and the inherent three-dimensional models is enhanced on the deformation of a few of elements adjacent to the indenter edges, it is not expected to cause any noticeable difference in the load–depth relationship. The model is illustrated schematically in Fig. 2. The modeled indenter was perfectly rigid. The contacting interface between the specimen and the indenter tip was assumed to be frictionless, because throughout preliminary simulations the frictional force induced with friction coefficients up to 0.3 had few effects on the load–depth relationship. The mesh size was given to be sufficiently fine to keep accuracy: the minimum element size was 0.05 μm. The total number of the elements used in the model was 1509. The loading rate in the calculation is small enough to neglect an inertia effect as static condition.

The constitutive model of the ceramic specimen material before immersion was that of an elastic–plastic von Mises material with isotropic hardening: elastic–perfectly plastic with no strain hardening. The validity of these vales was confirmed through the inverse analysis on the substrate.

4. Results

4.1. Changes of mass, hardness and strength

Fig. 3 plots the changes of mass, hardness and strength to immersion time, using normalized values: M/M_0, H/H_0, σ/σ_0. Except for ZrO_2, there was not considerable mass change throughout the immersion test up to 1000 h. In particular, the mass change of Si–SiC was hardly recognized, while the mass of ZrO_2 reduced to about 60% by 10 h-immersion in the boiling sulfuric acid. The hardness is more sensitive to the immersion time than the mass. Despite the kind of the ceramics the corroded surfaces tend to become softer as the immersion time increases.

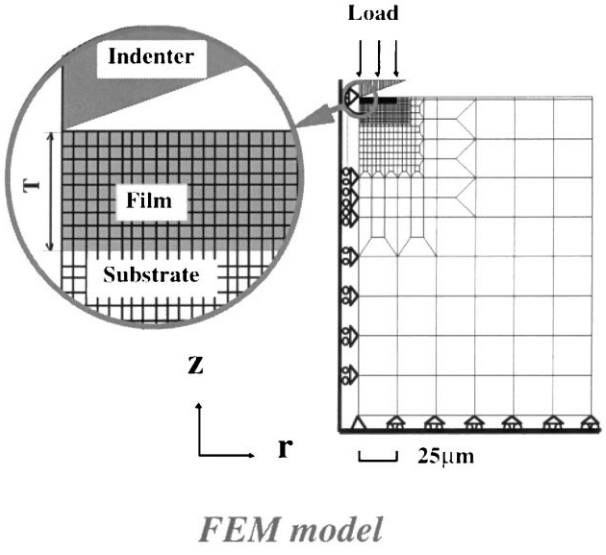

Fig. 2. FEM model for indentation simulation.

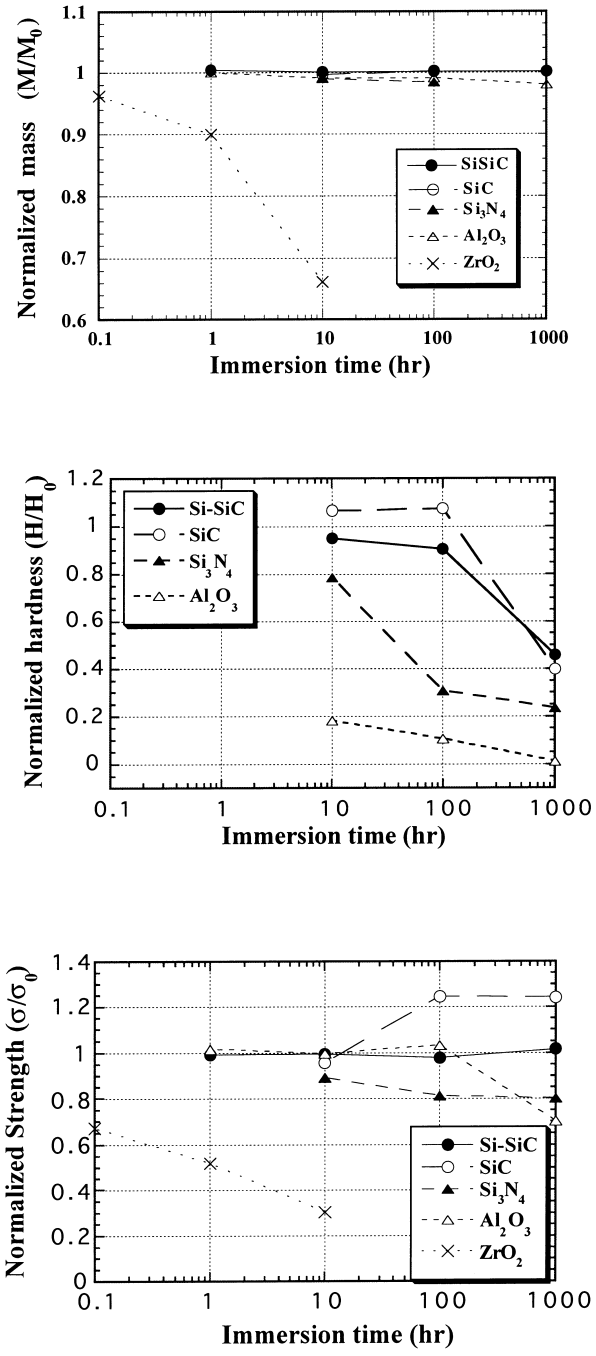

Fig. 3. Relationship between immersion time and changes of mass, hardness and strength.

The three-point bending strengths of the specimens were obtained after being immersed for each period. The strength of SiC increased by about 20% after the immersion for more than 100 h. The corrosion due to the boiling sulfuric acid has little effect on the strength of Si–SiC. On the other hand, the strengths of Al_2O_3, Si_3N_4 and ZrO_2 decreased after the immersion: that of ZrO_2 was remarkably degraded after only a few minutes immersion, those of Al_2O_3 and Si_3N_4 decreased by about 20% after 1000 h immersion. Except for ZrO_2, the relationship between the mass change and the strength degradation is unclear unlike conventional metals. The strength of brittle materials is very dependent on the surface condition: roughness and/or flaws on the surface. Since the hardness of corroded surface is considered to be associated with the strength, the results in Fig. 3 are replotted in Fig. 4 as a relationship between the hardness and the strength. Fig. 4 indicates the tendency that the larger the hardness the lower the strength becomes in the cases of SiC and Si–SiC, whereas the higher the strength in the cases of Si_3N_4 and Al_2O_3. The hardness may be an applicable parameter to indicate the strength degradation of brittle materials due to corrosion. Corroded surface appearance related to the hardness change will be discussed in Section 4. 3 in detail.

4.2. L/D–D *curve*

Fig. 5 shows representative relationships between load/depth and depth, L/D–D curve, on Si–SiC, Al_2O_3 and Si_3N_4 obtained after 100, 1000 h immersion. In the cases of Si–SiC, the curves during loading might be divided into two stages, i.e. 1st stages up to around 0. 15 μm for 100 h and around 0. 30 μm for 1000 h. The slope of the curve in the 1st stage is lower than that in the 2nd stage. Hereafter, the depth at which the transition from the 1st to the 2nd stages occurs is defined as d. The curves exhibit almost the same slope at the 1st stage regardless of the immersion time although the slope at the 2nd stage is affected by the immersion time.

The SiC exhibited the same trend as the Si–SiC. In the case of Al_2O_3 also divided into two stages, but the slope at the 1st stage is affected by the immersion time: the slope decreases with an increase of immersion time. In the case of Si_3N_4 in 1000 h immersion, the curve is divided into three stages. The slope of the 2nd stage is lower than that in the 1st and 3rd stages. In Section 4.3 discussion will be made in detail on the relationship between the d-value and corroded surface appearance and thickness.

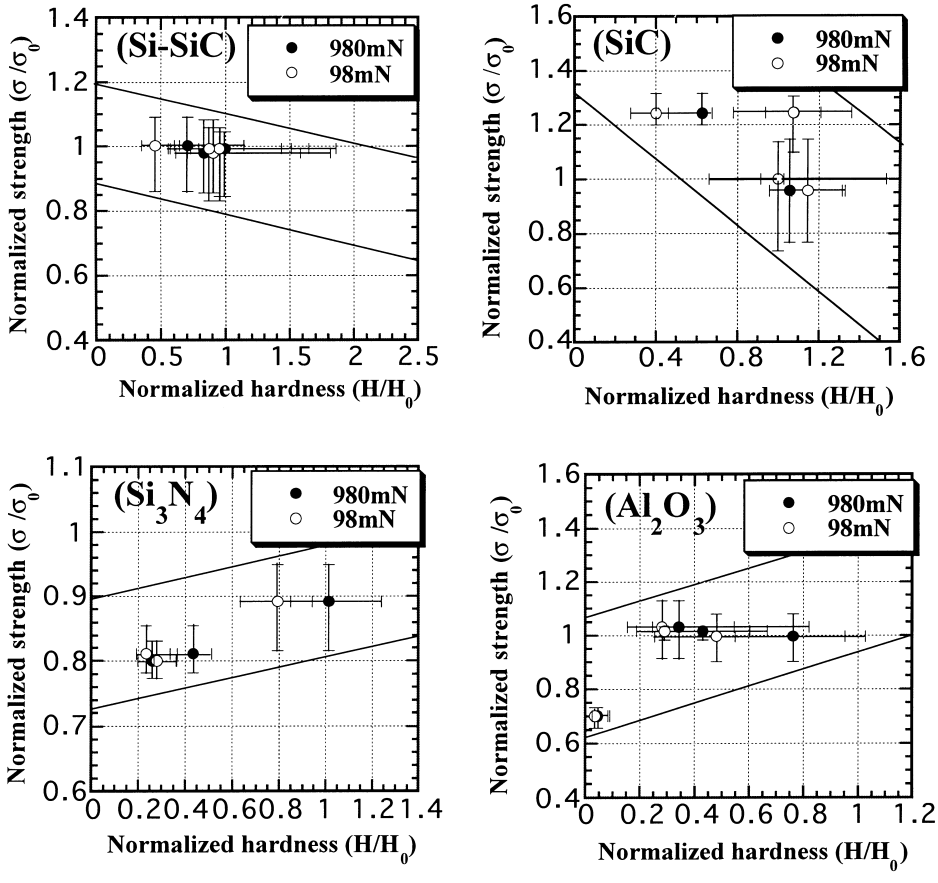

Fig. 4. Relationship between normalized hardness and strength.

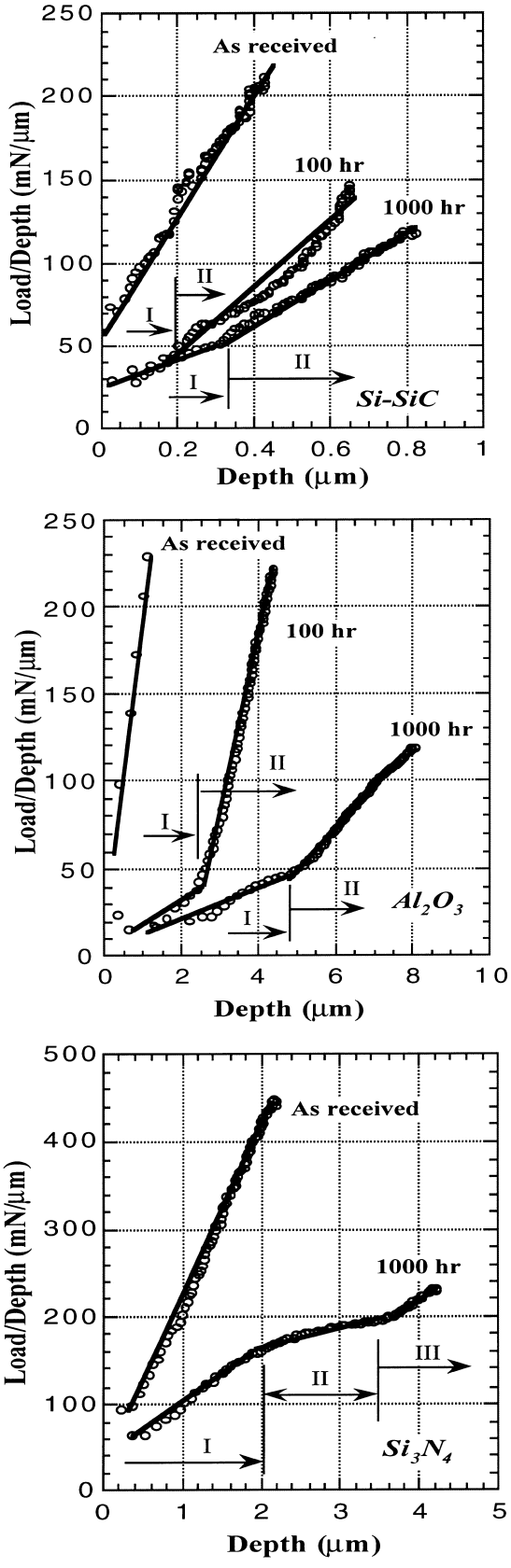

Fig. 5. Load/depth–depth curves of Si–SiC, Al_2O_3, Si_3N_4. The curves are divided into some stages: two stages in Si–SiC and Al_2O_3, and three stages in Si_3N_4.

4.3. Corroded layer appearance

Surface condition was investigated through SEM observation for the fracture surface to give interpretation for the L/D–D curve behavior. Fig. 6 shows the typical fracture surfaces of Si–SiC, Al_2O_3 and Si_3N_4 after 1000 h immersion. The formation of films was observed on Si–SiC surfaces. The film thickness of Si–SiC measured from SEM observation is about 1.4 μm for 100 h and 2.6 μm for 1000 h. The EPMA analysis indicating that main compositions of the film are O and Si and the ratio of atom concentration, O/Si, is 2/1, implies the silica film formation. Also, the observation for SiC exhibits the silica film formation as the Si–SiC.

It is seen from the fracture surface of Al_2O_3 with the EPMA line profile on S and Al that the corroded layer

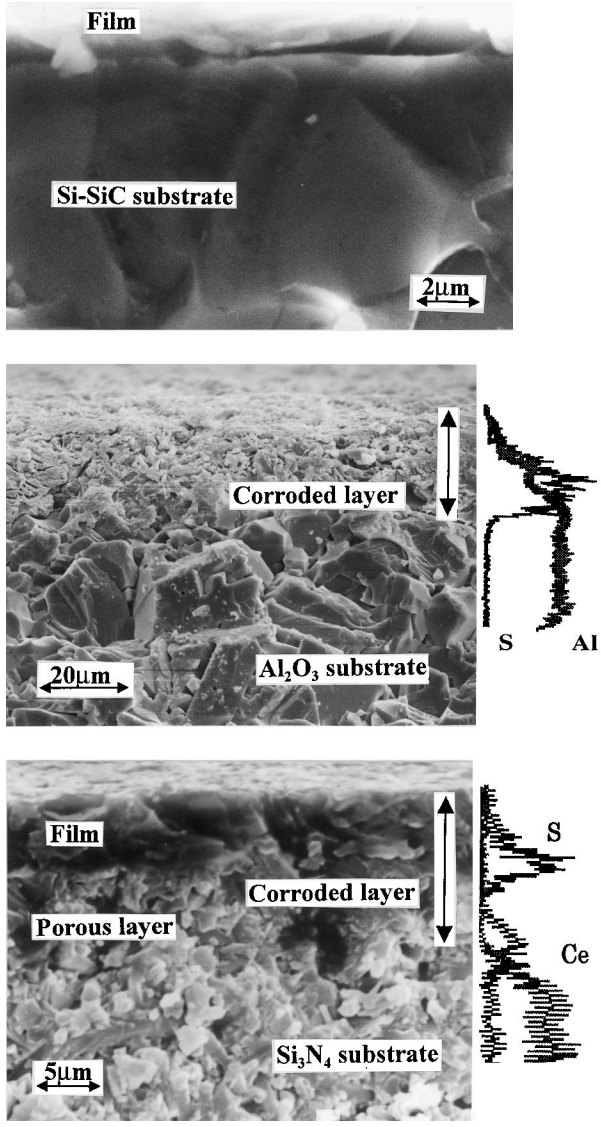

Fig. 6. Fracture surfaces including corroded layers after 1000 h immersion. In Si-SiC film formation, in Al_2O_3 gradient corroded layer formation, in Si_3N_4 corroded layer consisting of film and porous layers.

without any film scale generates in the surface area where the grain boundary becomes unclear due to intergranular attack. Amount of Al in the surface layer is less than that in the substrate because of Al dissolution into the sulfuric acid. Additionally, the presence of S including in the solution is recognized in the surface layer. The thickness of the corroded layer, therefore, was determined to be about 17 μm for 100 h and 50 μm for 1000 h immersion, taking account of the content change of the Al and S in the surface layer.

In the case of Si_3N_4, the layer with a relatively flat fracture surface was present close to the specimen surface and a porous layer beneath it. Since the main compositions of the flat layer are Si and O, the silica film forms on the specimen surface as Si–SiC. According to the EPMA line profile on S and an additive Ce, S exists in the corroded layer and the amount of Ce decreases in it. It is deduced that Ce was liquated out and S permeated into the porous layer. That is, the corroded layer consisting of the silica film and the porous layer was formed. The thickness of the corroded layer increase with the immersion time: about 10 mm for 100 h and about 20 μm for 1000 h immersion, including the silica film of 2 and 6 μm thickness, respectively.

Fig. 7 shows the relationship between the thickness of film T_f and corroded layer T_c, obtained from the SEM observation and the *d*-value of *L*/*D*–*D* curve. The *L*/*D*–*D* curve was fitted to a polynomial of the 6th order to quantitatively evaluate the *d*-value indicating the slope changing depth. The Si_3N_4 has two *d*-values associated with the formation of film and porous layer: one at the transition from the 1st and the 2nd stages and another from the 2nd and the 3rd stages. The latter is adopted as the *d*-value of the corroded layer in Si_3N_4. It is recognized that the relationship between *d* and $T_{f,c}$ is described as $T_{f,c} \approx 10d$, except for the range of $d < 0.2$ μm in the film. We will discuss the relationship in detail through the inverse analysis on the *L*/*D*-*D* curve in 5. 1

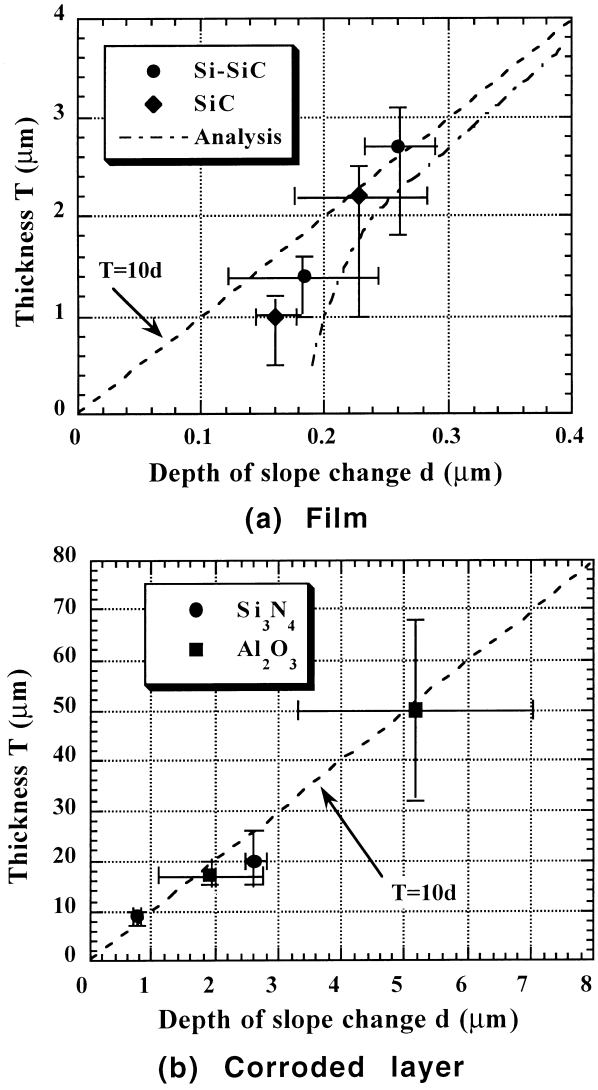

Fig. 7. Relationship between the *d*-value obtained from *L*/*D*-*D*-curve and thickness of film and corroded layer. In the film thickness less than 0.2 mm, the tip roundness effect is recognized.

5. Discussion

5.1. Inverse analysis on L/D-D curve

The inverse analysis on the *L*/*D*-*D* curve contributes to understanding of the *L*/*D*-*D* behavior and to estimation of mechanical properties of the film and the corroded layer: Young's modulus and yield stress. We categorized the corroded-layer formation into three types: the film formation: Si–SiC, SiC, the gradient porous layer formation; Al_2O_3, and the film and porous layer formation; Si_3N_4, as illustrated in Fig. 8. For the inverse analysis, in the case of the SiC and Si–SiC, the elastic properties of silica scales evaluated by micro-indentation method[8] were adopted as the properties of the film. In the case of the Al_2O_3, we assumed that the property correspond to the Al composition increasing gradually with the depth from the surface, as taking account of the EPMA line profile shown in Fig. 6. The corroded layer has the graded properties: *E* is varied from 4 GPa near the surface to 270 GPa near the subatrate and σ_y from 0.4 to 2.9 GPa, as tabled in Fig. 8. In the case of the Si_3N_4, the properties of the film formed on the surface are the same as the silica scales of Si–SiC and SiC. As for the properties of the corroded layer between the silica film and the substrate, we determined them after iterating a number of calculations to reach a suitable coincidence between analytical and experimental results on the *L*/*D*–*D* curves. Mechanical properties evaluated for the film and corroded layers are tabled in Fig. 8, respectively. Fig. 8 shows the comparison between experimental and analytical results on the

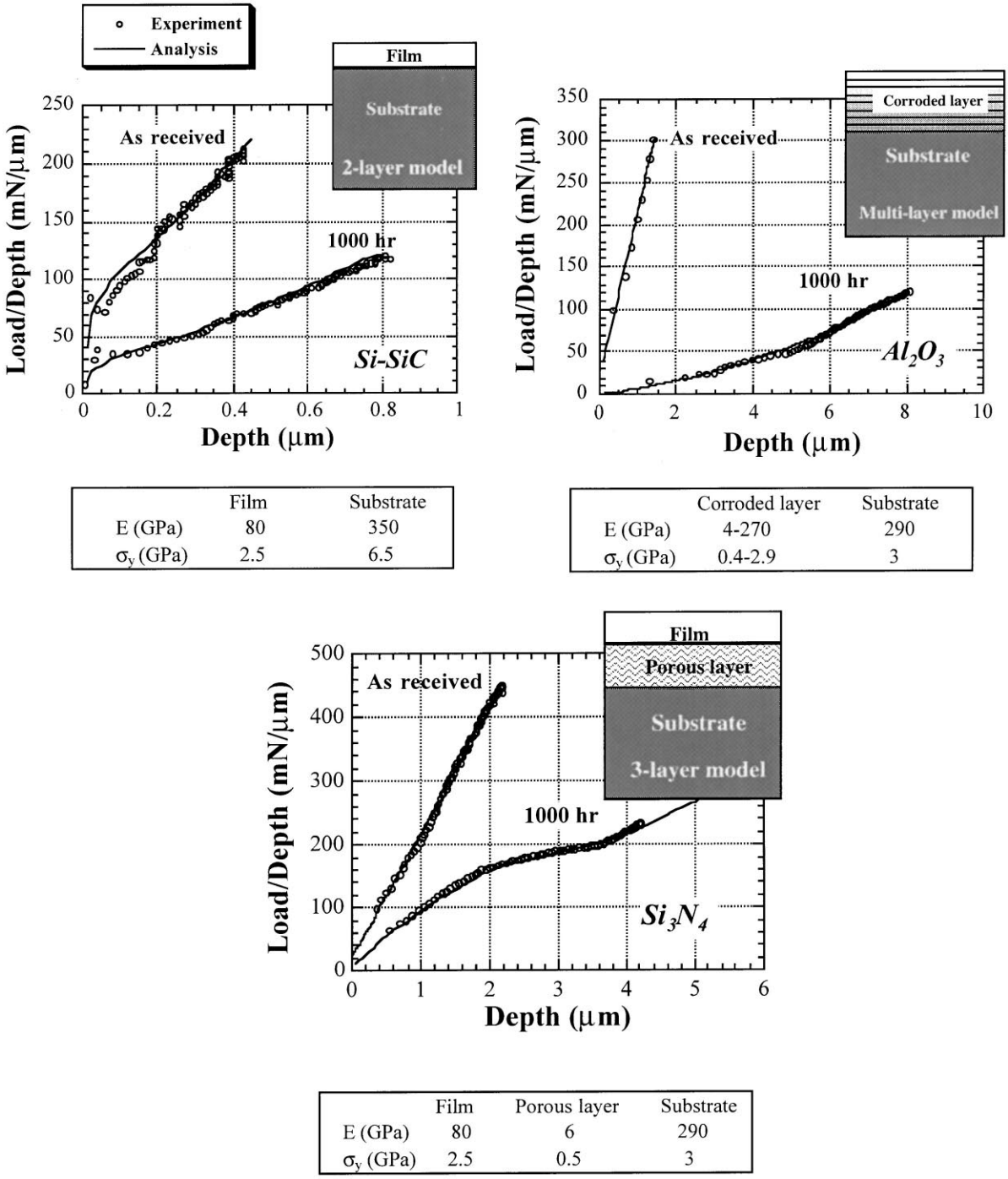

	Film	Substrate
E (GPa)	80	350
σ_y (GPa)	2.5	6.5

	Corroded layer	Substrate
E (GPa)	4-270	290
σ_y (GPa)	0.4-2.9	3

	Film	Porous layer	Substrate
E (GPa)	80	6	290
σ_y (GPa)	2.5	0.5	3

Fig. 8. Comparison on L/D–D curve between experimental and analytical results. Corroded layer models are shown in figures. Evaluated properties of layers are tabled.

L/D-D curves. The analytical results give good agreement with the experimental ones. Fig. 9 illustrates an example of the deformation and the maximum principal stress under indenter obtained from the FEM inverse analysis in the case of Si–SiC. When the d is smaller than $T_f/10$, the stress hardly imposes on the substrate and the indent load is not affected by the substrate. While, if the d becomes larger than $T_f/10$, the maximum stress appears in the substrate so that the L/D–D curve is definitely affected from the substrate. It can be said through the inverse analyses that when an indentation is made on the film and/or the corroded layer attached to a substrate having different elastic and plastic properties, the slope of the curve reflecting the indentation process is expected to change due to the gradually increasing influence of the substrate.

Additionally, if the thickness of film is small, influence of the roundness of the indenter tip can not be ignored

as the silica films formed on SiC and Si–SiC substrates seen in Fig. 7. In the analysis the tip radius was changed from 0∼3. 0 μm. The deviation from the relationship of $T=10d$ appeared at larger depth as the tip radius increased. The analytical results using $r=1.5$ μm describe appropriately the experimental ones as shown in Fig. 7. The tip radius measured experimentally with a laser microscope was about 1.5 μm. The analytical results shown in Fig. 8, therefore, take the 1.5 μm tip radius into account and give good agreement with experimental ones. It is confirmed that the micro-indentation technique combined with inverse analyses enables us to estimate the mechanical properties of the corroded layers and particularly the corroded depth which is associated with the strength degradation due to corrosion.

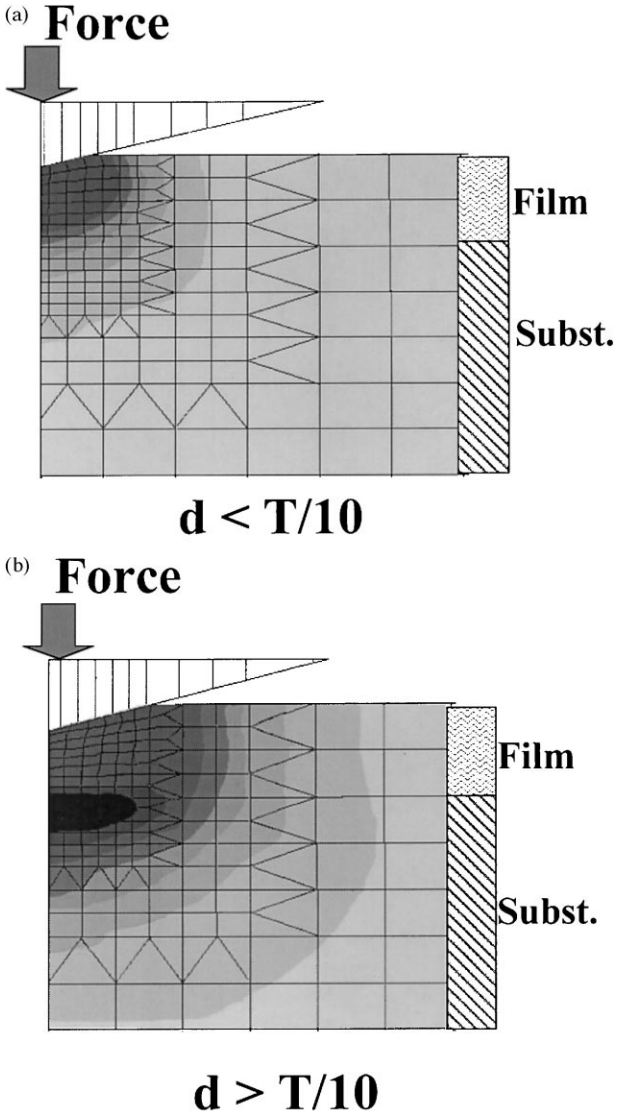

Fig. 9. Deformation and maximum principal stress distribution under indenter in the case of Si–SiC: (a) $d<T/10$; (b) $d>T/10$.

5.2. Evaluation of strength degradation

One of the objectives of this work has been to relate the microindentation technique with the corrosion damage evaluation. The important information given by the microindentation technique is the corroded depth and the film thickness, which may be used to quantify the corrosion damage. In the cases of Al_2O_3 and Si_3N_4, the relationships between the slope change depth d and the fracture strength for each immersion time were plotted in Fig. 10. The fracture strength is strongly associated with the corroded surface condition. [9,10] Assuming that the corroded layer is the surface flaw which causes crack propagation to fracture, the equivalent crack length to the surface flaw is given by:

$$a_e \approx T_c \approx 10d \tag{2}$$

We then tried to quantitatively evaluate the strength degradation of Si_3N_4 and Al_2O_3 using the relationship between an equivalent crack length a_e and an intrinsic fracture toughness K_{IC}, given by:

$$a_e = \frac{(K_{IC}/1.12\sigma)^2}{\pi}, \tag{3}$$

assuming a surface edge crack.[11] The relationship between the equivalent crack length and the fracture strength was described as a line drawn in Fig. 10, using Eq. (3) and K_{IC} in Table 1. Except for Si_3N_4 in 1000 h immersion, it is found that the strength degradation was adequately evaluated by using Eq. (3) and the relationship between a_e, T and d is describable by Eq. (2) and the strength degradation due to corrosion is nondestructively

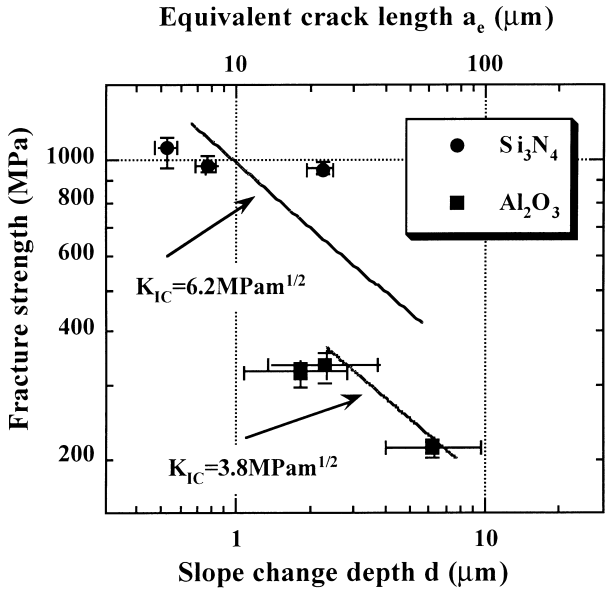

Fig. 10. Fracture strength of Si_3N_4 and Al_2O_3 as a function of equivalent crack length calculated from depth of slope change d.

evaluated by using the microindentation technique. The strength of Si_3N_4 after 1000 h immersion, at $a_e \approx 20$ μm, is higher than the line given by Eq. (3). This seems to be because the film formation above the porous layer in Si_3N_4 has a function to strengthen:[12] the thickness of the film after 1000 h immersion reaches to about a third of the corroded layer.

6. Conclusion

The instrumented depth-sensitive microindentation technique was applied to evaluate mechanical properties on the thin corroded layers of ceramic materials which were immersed in boiling highly condensed sulfuric acid up to 1000 h. The indentation load–depth curves were analyzed using a finite element model to investigate the effect of the film or the corroded layer on the curves. The main conclusions are summarized as follows:

1. The corrosion behaviors of these ceramic materials were divided into three types: (1) Si–SiC and SiC exhibited excellent corrosion resistance because of the protective oxide film formation during immersion; (2) the bending strength of Si_3N_4 and Al_2O_3 decreased with increasing immersion time because of the corroded layer formation; (3) the bending strength of ZrO_2 decreased with remarkable weight loss.
2. The thickness T of the corroded layer was evaluated from the depth d which is determined by the slope change of the L/D–D curve.
3. The mechanical properties of both the oxide films and the corroded layers were evaluated on the basis of analytical and experimental results on the indentation curves. Then, it was confirmed that the relationship between the thickness T of both oxide films and corroded layers and the depth d is described as $T \approx 10d$.
4. The bending strengths of Si_3N_4 and Al_2O_3 after the immersion were evaluated using both the d associated with the corroded layer thickness and the K_{IC} obtained before immersion. As a result, it was found that the strength degradation of Si_3N_4 and Al_2O_3 due to the boiling sulfuric acid corrosion can be estimated with both the K_{IC} and the d-value.

Acknowledgements

The authors would like to thank Mr Fukaya of Japan Atomic Energy Institute for SEM observation and Mr Nishiyama of Ishikawajima-Harima Heavy Industries Co., Ltd for experiment.

References

1. Onuki, K., Nakajima, H., Ioka, I., Futakawa, M. and Shimizu, S. IS-process for thermochemical hydrogen production. *JAERI-Review* 94-006, 1994.
2. Onuki, K., Nakajima, H., Ioka, I., Futakawa, M., Nakajima, H., Shimizu, S. and Tayama, I., Screening tests on materials of construction for the thermochemical IS process. *Corrosion Engineering*, 1997, **46**, 141–149.
3. Lay, L. A., *Corrosion Resistance of Technical Ceramics*. HMSO, London, 1991.
4. Frechette, V. D., *Failure Analysis of Brittle Materials*. Advances in Ceramics. The American Ceramic Society, Vol. 28, 1990.
5. Murakami, Y. et al., *Stress Intensity Factors Handbook*, Vols. 1 and 2. Pergamon, 1987.
6. Inamura, M. and Suzuki, T., Evaluation of material strength by ultra-micro-indentation. *Seisankennkyu*, 1990, **42**(4), 257–260in Japanese.
7. Hallquist, J. O., *LS-DYNA Theoretical Manual*. Livermore Software Technology Corporation, 1993.
8. Futakawa, M. and Steinbrech, R. W., Elastic/plastic properties of bilayered silica scales on SiC. In *Proceedings of the 5th European Conference on Advanced Materials and Processes and Applications*, ed. L. A. J. L. Sartan and H. B. Zeedijk. Netherlands Society for Material Science, Zwijndrecht, Netherlands, 1997, pp. 377–380.
9. Smialek, J. L. and Jacobson, N. S., Mechanism of strength degradation for hot corrosion of α-SiC. *J. Am. Ceram. Soc.*, 1986, **69**(10), 741–752.
10. Arai, M. and Kohno, A., Corrosion behavior of sintered silicon nitoride ceramics in acid and alkaline solutions. *Zairyo-to-Kankyo*, 1995, **44**, 276–280 in Japanese.
11. Koiter, W. T., *Trans. ASME, Ser. E*, 1965, **32**, 237.
12. Futakawa, M., Onuki, K. and Steinbrech, R. W., Corrosion resistance of oxide scale formed on SiSiC in boiling sulfuric acid. *Hyomen Gijyutu*, 1997, **48**(6), 662–663 (in Japanese) .